Environ. Sci. Technol. **2007**, *41,* 2289−2295

Efflorescence Transitions of Ammonium Sulfate Particles Coated with Secondary Organic Aerosol

SATOSHI TAKAHAMA,[†]
RAVI K. PATHAK,[†] AND
SPYROS N. PANDIS*[,†,‡]

Department of Chemical Engineering, Carnegie Mellon University, Pittsburgh, Pennsylvania 15213, and Department of Chemical Engineering, University of Patras, Patra GR 26500, Greece

Ammonium sulfate particles were generated by atomization and introduced into a smog chamber where they were coated with secondary organic aerosol from ozonolysis of limonene or α-pinene. These mixed particles were then sampled with a humidified Tandem-DMA system where a monodisperse aerosol population was selected, humidified, and dried to observe the relative humidity (RH) at which the particles returned to the original dry diameter. The volume fraction of secondary organic aerosol (SOA) in the mixed particles ranged from 0.59 to 0.94 for limonene SOA and 0.54 to 0.72 for α-pinene SOA. Efflorescence RHs for our mixed aerosols were in the range of 28−34%, similar to our observation of 32% ERH for pure ammonium sulfate nanoparticles. These findings indicate that the effect of SOA on the ERH of inorganic salts in the atmosphere may be negligible.

Introduction

Fine particles in the atmosphere are comprised of sulfate, ammonium, nitrate, elemental carbon, organic material, trace metals, crustal elements, and water. Water can account for a large fraction of the aerosol mass in the atmosphere (*1*), and its uptake is dependent on the particle chemical composition and meteorological conditions. Phase transitions in particles from liquid to solid (and vice versa) can introduce further complexities by introducing discontinuities in the hygroscopic properties of aerosols.

Aerosols commonly exhibit a hysteresis effect in water uptake and growth following changes in relative humidity (RH) (*1*). For example, when the ambient RH around a solid ammonium sulfate particle is increased, the particle will begin to absorb water rapidly above a threshold RH known as the deliquescence RH (DRH). Upon decreasing the RH around a liquid ammonium sulfate particle, however, the particle will often remain liquid below the DRH. Solid-phase nucleation is not observed until a critical supersaturation is reached, at what is typically known as the efflorescence RH (ERH). Since a typical lifetime of an aerosol in the atmosphere is on the order of several days, this complicates the prediction of the aerosol's phase-state as it undergoes extreme changes in RH in the atmosphere. Field studies have shown that particles can exist in a deliquesced or effloresced state or as metastable aerosols in the atmosphere (*2*).

* Corresponding author e-mail: spyros@andrew.cmu.edu.
† Carnegie Mellon University.
‡ University of Patras.

The ability to predict the phase state of the aerosol has many implications on a regional and global scale. For instance, the phase state of the aerosol affects its optical properties; Martin et al. (*3*) showed that this effect can make a difference on the global annual average of calculated direct radiating forcing by approximately 25%. Whether there is liquid present or not in the aerosol also changes heterogeneous reaction kinetics and mechanisms. The hydrolysis of N_2O_5, a key reaction in nitric acid production during the night, has been shown to proceed at least an order of magnitude faster on aqueous particles than on their solid counterparts (*4*). Furthermore, the phase-state of the particle can affect the partitioning of semivolatile species such as nitric acid (*5*). When this partitioning effect is coupled with removal by dry deposition, the difference in phase-state can make a difference in inorganic $PM_{2.5}$ mass predictions by as much as 50% (*6*). Rees et al. (*7*) found that acidic particles conditioned at the RH specified by the Federal Reference Method may not in fact be effloresced; in these cases, water will bias estimates of "dry" $PM_{2.5}$ mass and complicate the regulation of fine particulate matter. Therefore, understanding phase transitions in atmospheric particles remains a priority.

There has been significant progress in understanding the DRH of multicomponent inorganic (*8*) and mixed inorganic/organic aerosols (*9*), and the corresponding models are in development. The ERH, however, is governed by kinetics and has proved difficult both to measure and to predict. Efflorescence is sensitive to the composition of the aerosol, particle size, drying rate, and the presence of foreign substances that can act as nuclei for nucleation, among other factors (*2*). Nucleation of the solid phase is rationalized by random collisions within a liquid phase producing a cluster of molecules of critical size (the germ), and subsequently molecules from the liquid phase break liquid−liquid bonds and form liquid−solid bonds (*2*, *10*). The presence of foreign substances in the solution, known as heterogeneous nuclei, can lower the energy barrier to critical germ formation. Classical nucleation provides a framework for the treatment of these processes, but the theory relies on bulk-phase properties and planar surface free energies to characterize molecular-scale interactions (*11*). Independent measurements of these parameters are often unavailable and are instead derived from fitting procedures (*11*) that have large uncertainties. Nonclassical theories employ statistical approaches to simulate the solid-nucleation processes (*2*, *10*, *11*), but these approaches are still not rigorous enough for practical application in atmospheric sciences (*2*). At this current stage, there is no means by which the ERH can be estimated a priori for a wide range of chemical compositions and environmental conditions (*2*), and so laboratory experiments remain the best alternative to study the behavior of each individual system in question.

Laboratory studies investigating aerosols comprised of electrolyte solutions and mineral dusts have largely been able to present a consistent picture of these systems. For instance, Martin and co-workers (*12*, *13*) have examined the efflorescence of ammonium nitrate and ammonium sulfate with or without inclusions of insoluble mineral dust that provide sites for heterogeneous nucleation and confirmed that heterogeneous nuclei raise the ERH of inorganic aerosols. Martin et al. (*14*) also parametrized a multicomponent inorganic system of NH_4^+-NO_3^--SO_4^{2-}-H^+ at 293 K and determined that the ERH is higher for aerosols with a large fraction of ammonium sulfate, as opposed to ammonium nitrate or sulfuric acid.

10.1021/es0619915 CCC: $37.00
Published on Web 02/24/2007

Studies of inorganic aerosols each mixed with a single organic compound, on the other hand, have not resulted in a clear understanding of the influence of organics on the efflorescence of inorganic particles. Depending on the compounds chosen and even the initial phase-state of the organic component, researchers have found a wide range of effects on the particle ERH, and similar experiments were not necessarily in agreement with each other. For instance, Lightstone et al. (*15*) observed that if succinic acid was not entirely dissolved in an ammonium nitrate solution, the ERH of the aerosol increases from the case of pure inorganic aerosol with increasing mole fraction of the succinic acid. If the organic species was completely dissolved, however, no efflorescence was observed in the mixed ammonium nitrate/succinic acid particle. Choi and Chan (*16*) also found that inclusions of compounds of varying solubility such as succinic acid and glutaric acid in a 1:1 mole ratio with ammonium sulfate increased the ERH of the aerosol (from 37 to 40% to >40% for succinic acid and around 60% for glutaric acid). However, Pant et al. (*17*) present a contradicting observation to Choi and Chan (*16*) that inclusions of glutaric acid showed either similar or lower ERHs (average of 27 ± 3%) than pure ammonium sulfate (ERH of 30%), depending on the ratio of organics to inorganics. Garland et al. (*18*) also reported that their inclusion of an insoluble organic material had no effect on ammonium sulfate ERH for up to 45 wt % palmitic acid/55 wt % ammonium sulfate.

With the inclusion of more water-soluble organic components, the ERH of the inorganic aerosol appears to be lowered or not affected, though sometimes both effects were found for the same organic compound. The presence of citric acid (0.5 mole fraction) and oxalic acid (0.4 mole fraction) were shown to decrease the ammonium sulfate ERH by Choi and Chan (*16*) and Prenni et al. (*19*), respectively. Choi and Chan (*16*) found that glycerol did not have a significant effect on the ERH of ammonium sulfate, but Parsons et al. (*20*) found that it reduced the ERH as much as 30% up to an organic mole fraction of 0.6. In contradicting studies, however, Prenni et al. (*19*), Parsons et al. (*20*), Braban and Abbatt (*21*), and Hämeri et al. (*22*) found that malonic acid decreased the efflorescence of ammonium sulfate at organic mole fractions of 0.3, above 0.4, <0.6, and 0.5, respectively, while Choi and Chan (*16*) found that even at a 0.5 organic mole fraction, malonic acid did not have a significant effect on the ERH of ammonium sulfate. Brooks (*23*) found that for maleic acid, a compound similar in solubility to malonic acid, the ERH of ammonium sulfate (30%) was lowered only slightly (on average to 27 ± 3%) regardless of the proportion of each in the mixture.

Thus far, the hygroscopic properties of the pure organic components have not been a strong indicator of their influence on the ERH of ammonium sulfate. Many organics with lower or no efflorescence RHs affect the ERH of the inorganic component differently when included as internal mixtures. Therefore, it is almost impossible to predict what effect multicomponent organic mixtures as those found in the atmosphere might have on pre-existing inorganic aerosols.

To address this issue, we study the liquid-to-solid phase-transition properties of ammonium sulfate coated with ozonolysis products of two monoterpenes, α-pinene and limonene. Products of these reactions are known as secondary organic aerosol (SOA); the ubiquity of SOA in the atmosphere is well established. Cabada et al. (*24*) estimated that on average, 35% of the Pittsburgh aerosol may be SOA in composition; Lim and Turpin (*25*) estimated that the fraction could be as high as 88% in Atlanta. The oxidation products of the parent volatile organic compounds (VOCs) are numerous, and each individual component is expected to show a wide range of hygroscopic behaviors. The full extent of interactions of these species with inorganic aerosols has not yet been characterized. To this end, mixed particles comprised of ammonium sulfate and SOA are generated using the Carnegie Mellon University smog chamber and sampled with a humidified tandem differential mobility analyzer (HTDMA) to examine their efflorescence properties for a range of SOA to ammonium sulfate fractions.

Experimental Section

A schematic for the smog chamber and aerosol flow system is presented in Figure 1. Ammonium sulfate particles were generated by atomization, dried, and introduced into the smog chamber by positive pressure flow. These particles were then coated with condensable ozonolysis products of VOCs (limonene or α-pinene) and sampled with a humidified tandem differential mobility analyzer (HTDMA) system to observe their hygroscopic properties. Experimental conditions are described in Table 1. Two Scanning Mobility Particle Sizer (SMPS) units were employed during each experiment: one measured the evolution of the full size distribution in the smog chamber, and the other measured the hygroscopic growth of monodisperse particles at the terminus of the HTMDA.

Particle Generation. A 0.50 g/L or 0.88 g/L solution of ammonium sulfate (Sigma-Aldrich) prepared in distilled and deionized water (18.2 mΩ-cm resistance) was loaded into a syringe pump (kdScientific); 40−80 mL of this solution was pumped to a constant-output atomizer (TSI, Inc. Model 3076) at a rate of 2.5 mL/min. The particles were then dried in a diffusion denuder whose outer annulus was filled with silica gel, resulting in a output air stream with a RH less than 10%. Since the efflorescence RH of ammonium sulfate for this size range of particles is around 30%, this process resulted in a dry, polydisperse aerosol distribution with a geometric mean diameter of 75−80 nm, for solution compositions of either 0.50 g/L or 0.88 g/L.

Smog Chamber. The Carnegie Mellon smog chamber facility is described by Huff Hartz et al. (*26*). The chamber consists of a suite of instruments, including a 10 m^3 bag connected to five temperature sensors, one RH sensor (Vaisala HMK 233), UV bulbs, an ozone monitor (Dasibi Environmental Corp., Model 1008-PC), and an SMPS (TSI Model 3936). Though temperature controls were employed in some experiments, all of our studies were carried out in the absence of UV radiation.

The procedure of ozone and VOC injection in this smog chamber is described in detail by Huff Hartz et al. (*26*). Liquid VOCs stored in the freezer were transferred to a syringe and vaporized into the bag through a septum injector and a dry air source with bypass (*26*). The VOCs used in this experiment were limonene (Sigma-Aldrich) and α-pinene (Sigma-Aldrich), and the mixing ratios injected into the bag ranged from 5 to 50 ppb. An hour after initial seed injection, ozone was generated by corona discharge of an oxygen gas source. Ozone concentrations used in this study ranged from 500 to 600 ppb. In all experiments, 2-butanol was injected as an OH radical scavenger by volatilization of the liquid in a gas dispersion tube. The concentrations of 2-butanol ranged from 13 to 16 ppm. Table 1 summarizes the conditions of each experiment.

The particle size distribution was measured with a SMPS in recycle-mode (exhaust flow is recirculated back to the sheath airstream) and was operated at the same temperature as the chamber. The ozone concentration was recorded with an ozone monitor. The RH in the chamber during these experiments was 6−10%.

Humidified Tandem Differential Mobility Analyzer. Related HTDMA techniques have been described by several researchers (*19*, *27*−*29*). The aerosols in the bag are pulled by vacuum at a rate of 1.5 Lpm into a neutralizer (TSI) that

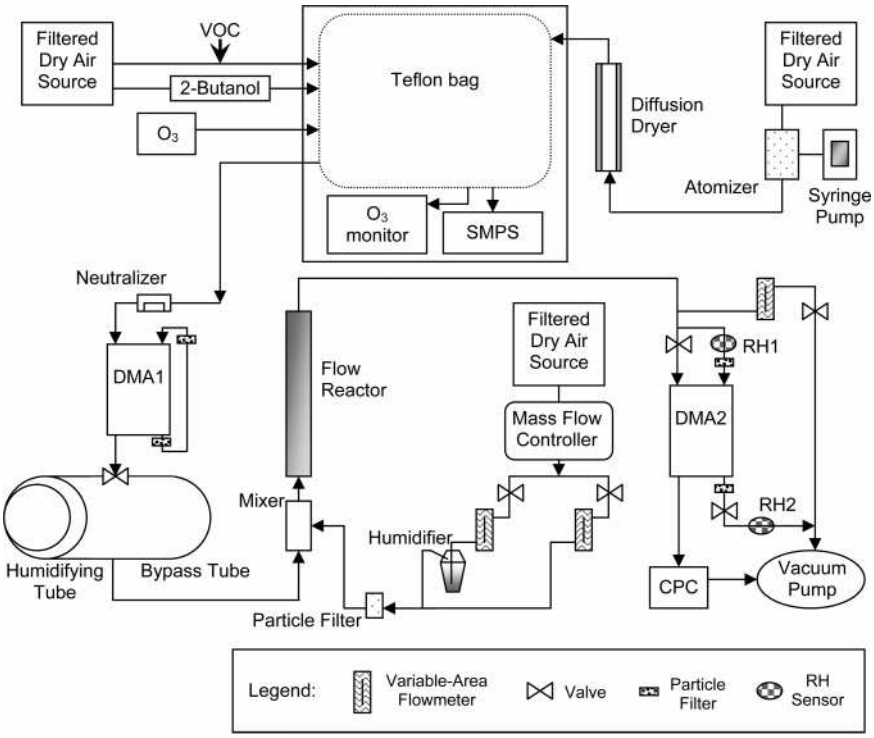

FIGURE 1. Diagram of the smog chamber and HTDMA flow system.

TABLE 1. Experimental Parameters

expt name	VOC	initial VOC mixing ratio (ppb)	smog chamber temp (°C)	initial O_3 concn (ppb)	distribution, final geom $\bar{D}_{p,V}$ (σ_{geo}) (nm)	particle size selected by HTDMA (nm)
L1	limonene	5	40	500	193 (1.8)	88
L2	limonene	5	30	500	181 (2.1)	105
L3	limonene	5	20	500	186 (2.4)	105
L4	limonene	50	40	500	212 (2.4)	107
L5	limonene	50	30	500	229 (2.6)	187
A1	α-pinene	8	25	500	176 (1.7)	133
A2	α-pinene	15	25	500	175 (2.1)	104
A3	α-pinene	23	25	600	182 (1.9)	137

confers a Boltzmann distribution of charges to the aerosols by a Kr-85 source. These particles are then selected by the first Differential Mobility Analyzer (DMA) according to their electrical mobility, which is determined by particle size and shape. The first DMA was operated much like the SMPS in the smog chamber; the exhaust flow was recycled to the sheath airstream (mass flow controllers and blowers of TSI Model 3080 were joined with column and high voltage source of TSI Model 3071A) at a rate of 15 Lpm. Particles between 80 and 190 nm were selected for each HTDMA experiment based on the size distribution of aerosols observed in the smog chamber.

The particles were then deliquesced in a humidifying tube (Perma Pure MH 110-48S-4), with a membrane permeable to water vapor separating sample airstream from the annulus of water around it. For a flow of 1.5 Lpm the dewpoint of the airstream exiting the tube is designed to be less than 1 °C lower than that of the airstream temperature, suggesting that the aerosols are humidified at an RH greater than 94%. As the deliquescence RH of ammonium sulfate is 80% and the DRH of mixed aerosols is lower by the mutual deliquescence argument (*30*), the particles that exhibit deliquescence behavior should be fully deliquesced upon exiting this tube.

To observe the efflorescence of these particles, the sample airstream is then mixed with an air stream of different RHs. The RH in the mixing stream is controlled by varying the ratio of wet air to dry air (dry air RH < 10%). Wet air is created by bubbling clean, dry air through a heated water bath; the temperature of this water bath is kept constant at 26 °C by a heating tape and PID controller (Omega CN76000). The total flowrate of the mixing air stream is kept constant at 6.5 Lpm by a mass flow controller (MKS 1179A) and the proportion of dry to wet air is adjusted manually with rotameter valves (Gilmont Accucal). The particles are then passed into a flow reactor with a volume of about 1 L, which gives an additional residence time of about 9 s before measurement of size by SMPS (TSI Model 3936). An optional line is also included upstream to bypass the humidifying tube to study the impact of water vapor on nondeliquesced particles.

An additional exhaust line just before the SMPS provides a means to balance the flows of the mixing stream, sample stream, and the SMPS, by adjustment of a rotameter valve. Just before the SMPS, the remaining airstream is split into the sample flow (1 Lpm) and the sheath flow (6 Lpm). An RH sensor (Vaisala HMK 233) and particle filter is placed in the sheath flow before the air enters the SMPS. The sheath flow must be at the same RH as the sample flow so that the particle does not take up or evaporate water in the DMA column; this method ensures that the two streams are at the same RH. An additional RH sensor is placed at the outlet of the excess flow of the SMPS. Because the particle filters do not immediately equilibrate with the water vapor in the airstream, we look for convergence in the RH before and after the DMA to determine when the system has come to equilibrium, and it is only these data points that we examine in this study. Using the normalized particle number, for size bins reported by the SMPS software (TSI, Aerosol Instrument Manager Software v5.2), we estimate the peak diameters using a cubic smoothing spline in R (*31*).

Estimation of SOA Volume Fraction of Particles. The volume fraction of SOA in the aerosol particles gives us a

measure of how much deviation from pure ammonium sulfate behavior we might expect, and this variable is estimated by two methods: (1) a bulk approach and (2) a size-resolved condensation-model calculation.

The bulk organic volume fraction is estimated from the size distributions of particles in the smog chamber. The size distribution of ammonium sulfate seed is measured with the SMPS until VOC injection and O_3 injection, and after this time the SMPS will measure the size distribution of ammonium sulfate plus SOA. The difficulty in estimating the SOA fraction from the difference in total volume concentration of aerosol before and after SOA formation and condensation is that particles are continuously being lost to the walls during this process. To account for this deposition loss, we assume that the total volume of particles follows a first-order loss process. The details are described in ref *32* and are also summarized in the Supporting Information.

Ozonolysis reactions of monoterpenes form semivolatile products and proportionally condense onto the size-range of particles that collectively offer the highest available surface area. Particle sizes sampled with the HTDMA were less than or equal to the peak diameter of the number size distribution in the smog chamber because the size-resolution of the DMA is finer for smaller diameters, giving better resolution in size changes. Because SOA preferentially condenses onto smaller particles on account of their available surface-area, the bulk SOA volume fractions can therefore be viewed as lower bounds for the volume fraction of SOA in particles studied by the HTDMA. We use information about the observed changes in total volume of particles and employ a one-product condensation model to separate the inorganic and organic contributions to the monodisperse population of aerosols selected for study. The condensation of material on seed particles of the same composition (ammonium sulfate) together with the relatively fast mixing time scale of the smog chamber (of the order of a minute or less) leads to internally mixed particles, that is all particles of the same size will have the same chemical composition. Details of the calculations are described in the Supporting Information.

Calculation of Efflorescence Relative Humidity. We estimate the efflorescence RH as the RH at which the humidified size distribution becomes statistically indistinguishable from the dry size distribution. Because we cannot be certain that no water has been retained by the particles after drying, this will be an "effective" ERH estimate. The details of the method are as follows. First, n dry diameter measurements at low RH are used to establish a mean diameter, $\bar{x}$, and its corresponding standard deviation, s. The limit of detection, L_D, is then calculated as

$$L_D = \bar{x} + t_{1-\alpha,\upsilon} \cdot s/\sqrt{n}$$

where $t_{1-\alpha,\upsilon}$ is the value of the student's t-distribution for a confidence level of $\alpha = 0.95$ and $\upsilon = n - 1$ degrees of freedom. We then perform a test of hypothesis to determine if the humidified peak diameters are above this limit of detection; those that are greater than the specified threshold are assigned to one category, and those below to another. After having transformed a continuum of peak diameters into a set of binary data, we fit a logistic regression model that has the following form

$$\text{logit}(p_i) = \ln\left(\frac{p_i}{1 - p_i}\right) = \beta_0 + \beta_1 \text{RH}_i$$

where p_i is the probability of observing a size distribution with a peak larger than the dry diameter (at the given RH_i), $\text{logit}(p_i)$ is its logit transformation (*33*)—the natural log of the probability that the particles are wet rather than dry—and β_0 and β_1 are regression parameters. Logistic regression is a subclass of generalized linear models, in which the random component of the predictor-response relationship can be modeled by a non-normal distribution function (in this case, the binomial distribution) (*34*, *35*). The information we can obtain from this regression model is the probability of observing efflorescence at a given RH; the probability can also be interpreted as the number of observations of nondry aerosol distributions in N number of trials generated by a Bernoulli sequence (*33*−*35*). This regression model captures the uncertainty arising from two distinct processes: (1) measurement and peak-fitting error and (2) the stochastic nature of crystal formation. The reported ERH and uncertainty is the median value and the bounds which encompass the 5th−95th probabilities. Figure 2 shows an illustration of this technique applied to our data. For data in which there is complete separation of the data in regions of 0's and 1's, the reported ERH is the mean between the lowest RH of particles classified as wet and the highest RH of the particles classified as dry. The associated uncertainties in these cases are reported as half the gap width or the combined RH sensor uncertainty, whichever is greater.

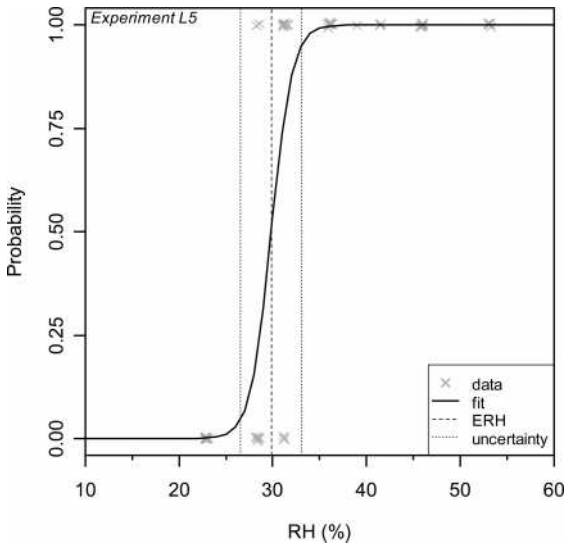

FIGURE 2. Illustration of logistic regression fit for estimating effective efflorescence relative humidity (ERH). Data points that lie at 0.00 probability indicate effloresced particles; data points that lie at 1.00 probability indicate wet particles. The uncertainty reflects the 5th−95th percentile probabilities of efflorescence estimated from the regression.

In addition, we employ a local regression technique (*36*) in the neighborhood of the ERH (20−50% RH) to locate an inflection point in the growth factor (GF) as a function of RH. The GF (*1*) is defined as the humidified diameter divided by the dry diameter and is indicative of the amount of water taken up by the particle. An efflorescence transition may be accompanied by a vertical discontinuity in GF, which, if present, would be represented by inflection in a smooth curve that approximates the data (*37*). Details are described in the Supporting Information.

Results and Discussion

Bulk SOA volume fractions in the smog chamber ranged from 0.30 to 0.81 for limonene SOA and 0.41 to 0.49 for α-pinene SOA. The size-resolved SOA volume fractions calculated by the condensation model are 0.59−0.94 for limonene and 0.54−0.72 for α-pinene for the particle sizes used. The model performs with a mean normalized error of less than 20% for the volume between 80 and 400 nm (relative errors outside of this range are biased by size bins with a negligible count of particles), except for experiments L4 and L5. In these two

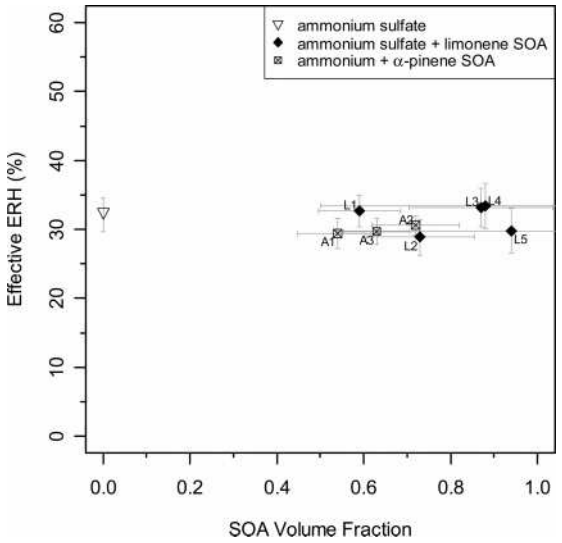

FIGURE 3. Effective efflorescence relative humidity (ERH) as a function of size-resolved SOA fraction of total ammonium sulfate + SOA aerosol. Labels next to data points indicate names of each SOA-generation experiment as described in Table 1. Vertical error bars indicate the 5th−95th percentile probabilities estimated for the ERH, and horizontal error bars reflect the magnitude of error in the fit of the condensation model for estimating the volume fraction.

experiments, the bulk SOA volume fractions exceeded 0.70 and were much higher than in the rest of the experiments. The estimation in our dry peak diameters is another potential source of uncertainty but is only on the order of 2% of the reported SOA volume fraction. Larger errors indicate that the one-product condensation model is not as accurate at these higher organic loadings; this introduces larger uncertainties in the size-resolved SOA volume fraction but not in the efflorescence RH.

Recent studies have indicated that pure SOA particles generally takes up less water than ammonium sulfate and do not exhibit an efflorescence transition (α-pinene + O_3, (*38*); 1,3,5-TMB + NO_x + OH + *hv*, (*39*); cycloalkene ozonolysis and sesquiterpene/monoterpene photooxidation products (*40*)). The ERH of pure ammonium sulfate particles of submicron diameters is reported in the range of 31−35% (*41*, *42*). The ERH of pure ammonium sulfate (dry diameter around 90 nm) estimated from our experiments is 32.1 ± 2.5%. Experiments conducted with larger particles (≥1 μm) may not be directly comparable, as their ERHs are systematically higher (33−37%) (*43*, *44*). The expectation time for the production of a crystalline germ follows Poisson statistics and is indirectly proportional to the system volume, leading to larger particles of equivalent chemical composition efflorescing at a higher RH (*2*).

The effective ERHs for ammonium sulfate coated with SOA (dry diameters of the mixed aerosols ranged from 80 to 190 nm) estimated—for all SOA volume fractions studied in our experiments and for both limonene and α-pinene ozonolysis products—ranged from 28 to 34%, in a range indistinguishable from pure ammonium sulfate (Figure 3). The effective ERH indicates the RH at which the humidified particle diameter became indistinguishable from its original dry diameter, as estimated from our hypothesis testing and logistic regression procedure. In employing a hypothesis-testing approach to disaggregate a continuous variable (peak diameters) into a binary variable (wet or dry), thresholds are often chosen to miminize Type I errors (in our case the error of mistakenly classifying dry particles as wet); the possibility still exists that we have misclassified wet particles as dry. To investigate this possibility we also used a local regression technique (*36*) that does not require a priori assumptions about the overall structure of the curve; we still find that inflection points in GF arise in all cases at RHs within the uncertainty of effective ERHs estimated from the logistic regression method. An inflection point in a smooth curve does not guarantee the existence of a discontinuity in the data it approximates, but a curve that approximates smooth hygroscopic growth of pure SOA (*40*) contains no inflection points—consistent with the observations of researchers (*40*) that no efflorescence behavior is seen in these aerosols. Thus, the fact that inflection points do arise in the curves obtained by the local regression method is suggestive of a transition and enforces the effective ERH as a relevant metric.

It is also possible for discontinuities to exist in a hygroscopic growth curve but to remain undetected during measurements of overall size distributions; Biskos et al. (*45*) observed that in ammonium sulfate nanoparticles the change in peak diameter with respect to RH near the ammonium sulfate transition point was gradual, suggesting the occurrence of nonprompt efflorescence. However, the researchers explained this phenomenon by assuming that the measured size distribution was a combination of two distributions in different proportions—one composed of the crystallized ammonium sulfate and the other composed of the wet particles (*45*).

Our effective ERH estimates are in agreement with Kleindienst et al. (*46*), who studied the relationship between RH and liquid water content of *p*-xylene, toluene, and 1,3,5-TMB photooxidation-generated SOA seeded with 20 $\mu g/m^3$ of ammonium sulfate. Using a liquid water content analyzer, the researchers found that for any of the three aromatic hydrocarbon precursors used to produce SOA, these mixed particles (organic mass fractions of 0.07−0.26, assuming mass organic-mass-to-organic-carbon ratios of 1.4) appear to completely dry out at around 30% RH—near the crystallization RH of ammonium sulfate (*46*).

Findings from our study regarding the effect of organics on ammonium sulfate efflorescence can be compared on a qualitative level with studies using larger particles; differences in system volumes discussed earlier limit the power of direct comparisons of absolute ERHs but not general trends. Our results are similar to observed effects of both soluble and insoluble organic compounds with varying hygroscopic behaviors mixed with ammonium sulfate: palmitic acid (*18*), maleic acid (*23*), glycerol (*16*), malonic acid (*16*), and humic acid (*47*). In contrast, other studies have reported ternary mixtures of ammonium sulfate, water, and an additional organic compound exhibit lower ERHs, and those in which a clear phase transition was not observed (malonic acid (*16*, *19*−*21*); citric acid (*16*); oxalic acid (*19*); and glycerol and levoglucosan (*20*)).

Suppression of crystallization presumably occurs in a mixture when additional molecules prevent the required supersaturation with respect to any of the original single-component solid phases to be reached in solution. Additionally, higher ERHs of ammonium sulfate have been reported when mixed with organics (succinic and glutaric acid (*16*), humic acid salts (*47*) at higher mass fractions); this might be attributed to the organics efflorescing first and inducing heterogeneous nucleation in the ammonium sulfate (*23*). It is also possible that a mixed salt consisting of ammonium sulfate and additional component(s) provides another pathway for germ formation, leading to a higher ERH. Our observations do not show evidence of such phenomena in our experiments. However, there is a possibility that since our SOA was generated in a dry environment (RH < 10%), insufficient time may have been available during humidification for dissolution and aqueous-phase diffusion to allow inorganic and organic species to interact. Other studies have found that upon efflorescence, the morphology of the dried particle may be such (e.g., solid shell containing trapped

liquid) that detectable amounts of water are retained at low RHs (*22*, *48*−*51*). As our dried particles returned to the initial dry diameter in our experiments, we consider such scenarios unlikely. However, the possibility remains that a small volume of water within the uncertainty of our dry diameter estimation is retained at the reported ERH—the size measurements of the HTDMA technique precludes direct observation of solid-phase nucleation. But our measurements suggest that the amount of water retained, if any, was small and that the RH at which the dried particles returned to the initial dry diameter was, within experimental uncertainty, the ERH of pure ammonium sulfate.

The α-pinene-O_3 reaction products characterized by Yu et al. (*52*) and limonene-O_3 reaction products characterized by Glasius et al. (*53*) indicate the formation and condensation of carboxylic acids, aldehydes, and hydroxyl aldehydes, spanning a range of solubilities in water (*26*, *54*). For the case of α-pinene ozonolysis for which Yu et al. (*52*) have provided measured yields of individual components, data indicate that mass fractions of any one product range from 0.01 to 0.3. The ERH of ammonium sulfate remains virtually unchanged when coated by a multitude of these organic compounds. These findings are informative for the purposes of predicting aerosol phase transitions. As previously mentioned, thermodynamic models are in development to predict the deliquescence and hygroscopic properties of mixed organic−inorganic aerosols (*9*); Martin et al. (*14*) have developed a parametrization for predicting efflorescence of inorganic components. If complex organic mixtures do not alter the efflorescence of the inorganic particles significantly, our current knowledge provides a strong basis for predicting the phase state of mixed particles in the atmosphere.

Acknowledgments

This was supported by NSF ATM-336296. The authors would like to thank P. Adams, C. Davidson, N. Donahue, K. E. Huff Hartz, and S. Martin for their discussions and assistance with the experiments.

Supporting Information Available

Calculation of bulk volume fraction and size-resolved volume fraction, estimation of inflection point by local regression, example size distributions, condensation model parameter description and values (Table S1), data analysis calculations and modeling results (Table S2), example comparison of modeled size distribution and measurement (Figure S1), regression model fitted to measurements (Figure S2), and size distributions as a function of RH (Figure S3). This material is available free of charge via the Internet at http://pubs.acs.org.

Literature Cited

(1) Seinfeld, J. H.; Pandis, S. N. *Atmospheric Chemistry and Physics*: *From Air Pollution to Climate Change*, 2nd ed.; John Wiley & Sons: New York, 2006.

(2) Martin, S. T. Phase transitions of aqueous atmospheric particles. *Chem. Rev.* **2000**, *100*, 3403−3453.

(3) Martin, S. T.; Hung, H. M.; Park, R. J.; Jacob, D. J.; Spurr, R. J. D.; Chance, K. V.; Chin, M. Effects of the physical state of tropospheric ammonium-sulfate-nitrate particles on global aerosol direct radiative forcing. *Atmos. Chem. Phys.* **2004**, *4*, 183−214.

(4) Thornton, J. A. B., C. F.; Abbatt, J. P. D. N_2O_5 hydrolysis on sub-micron organic aerosols: the effect of relative humidity, particle phase, and particle size. *Phys. Chem. Chem. Phys.* **2003**, *5*, 4593−4603.

(5) Ansari, A. S.; Pandis, S. N. The effect of metastable equilibrium states on the partitioning of nitrate between the gas and aerosol phases. *Atmos. Environ.* **2000**, *34*, 157−168.

(6) Vayenas, D. V.; Takahama, S.; Davidson, C. I.; Pandis, S. N. Simulation of the thermodynamics and removal processes in the sulfate-ammonia-nitric acid system during winter: Implications for PM2.5 control strategies. *J. Geophys. Res., [Atmos.]* **2005**, *25*, 2731−2748.

(7) Rees, S. L.; Robinson, A. L.; Khlystov, A.; Stanier, C. O.; Pandis, S. N. Mass balance closure and the federal reference method for PM2.5 in Pittsburgh, Pennsylvania. *Atmos. Environ.* **2004**, *38*, 3305−3318.

(8) Ansari, A. S.; Pandis, S. N. Prediction of multicomponent inorganic atmospheric aerosol behavior. *Atmos. Environ.* **1999**, *33*, 745−757.

(9) Clegg, S. L.; Seinfeld, J. H.; Brimblecombe, P. Thermodynamic modelling of aqueous aerosols containing electrolytes and dissolved organic compounds. *J. Aerosol Sci.* **2001**, *32*, 713−738.

(10) Pruppacher, H. R.; Klett, J. D. *Microphysics of Clouds and Precipitation*; Springer: New York, 1997.

(11) Laaksonen, A.; Talanquer, V.; Oxtoby, D. W. Nucleation: Measurements, Theory, and Atmospheric Applications. *Annu. Rev. Phys. Chem.* **1995**, *46*, 489−524.

(12) Martin, S. T.; Han, J. H.; Hung, H. M. The size effect of hematite and corundum inclusions on the efflorescence relative humidities of aqueous ammonium sulfate particles. *Geophys. Res. Lett.* **2001**, *28*, 2601−2604.

(13) Han, J. H.; Hung, H. M.; Martin, S. T. Size effect of hematite and corundum inclusions on the efflorescence relative humidities of aqueous ammonium nitrate particles. *J. Geophys. Res., [Atmos.]* **2002**, *107*, 4086.

(14) Martin, S. T.; Schlenker, J. C.; Malinowski, A.; Hung, H. M.; Rudich, Y. Crystallization of atmospheric sulfate-nitrate-ammonium particles. *Geophys. Res. Lett.* **2003**, *30*.

(15) Lightstone, J. M.; Onasch, T. B.; Imre, D.; Oatis, S. Deliquescence, efflorescence, and water activity in ammonium nitrate and mixed ammonium nitrate/succinic acid microparticles. *J. Phys. Chem. A* **2000**, *104*, 9337−9346.

(16) Choi, M. Y.; Chan, C. K. The effects of organic species on the hygroscopic behaviors of inorganic aerosols. *Environ. Sci. Technol.* **2002**, *36*, 2422−2428.

(17) Pant, A.; Fok, A.; Parsons, M. T.; Mak, J.; Bertram, A. K. Deliquescence and crystallization of ammonium sulfate-glutaric acid and sodium chloride-glutaric acid particles. *Geophys. Res. Lett.* **2004**, *31*, 4.

(18) Garland, R. M.; Wise, M. E.; Beaver, M. R.; DeWitt, H. L.; Aiken, A. C.; Jimenez, J. L.; Tolbert, M. A. Impact of palmitic acid coating on the water uptake and loss of ammonium sulfate particles. *Atmos. Chem. Phys.* **2005**, *5*, 1951−1961.

(19) Prenni, A. J.; De Mott, P. J.; Kreidenweis, S. M. Water uptake of internally mixed particles containing ammonium sulfate and dicarboxylic acids. *Atmos. Environ.* **2003**, *37*, 4243−4251.

(20) Parsons, M. T.; Knopf, D. A.; Bertram, A. K. Deliquescence and crystallization of ammonium sulfate particles internally mixed with water-soluble organic compounds. *J. Phys. Chem. A* **2004**, *108*, 11600−11608.

(21) Braban, C. F. A.; J. P. D. A study of the phase transition behavior of internally mixed ammonium sulfate-malonic acid aerosols. *Atmos. Chem. Phys.* **2004**, *4*, 1451−1459.

(22) Hameri, K.; Laaksonen, A.; Vakeva, M.; Suni, T. Hygroscopic growth of ultrafine sodium chloride particles. *J. Geophys. Res., [Atmos.]* **2001**, *106*, 20749−20757.

(23) Brooks, S. D.; Garland, R. M.; Wise, M. E.; Prenni, A. J.; Cushing, M.; Hewitt, E.; Tolbert, M. A. Phase changes in internally mixed maleic acid/ammonium sulfate aerosols. *J. Geophys. Res., [Atmos.]* **2003**, *108*, 10.

(24) Cabada, J. C.; Pandis, S. N.; Subramanian, R.; Robinson, A. L.; Polidori, A.; Turpin, B. Estimating the secondary organic aerosol contribution to PM2.5 using the EC tracer method. *Aerosol Sci. Technol.* **2004**, *38*, 140−155.

(25) Lim, H. J.; Turpin, B. J. Origins of primary and secondary organic aerosol in Atlanta: Results' of time-resolved measurements during the Atlanta supersite experiment. *Environ. Sci. Technol.* **2002**, *36*, 4489−4496.

(26) Hartz, K. E. H.; Rosenorn, T.; Ferchak, S. R.; Raymond, T. M.; Bilde, M.; Donahue, N. M.; Pandis, S. N. Cloud condensation nuclei activation of monoterpene and sesquiterpene secondary organic aerosol. *J. Geophys. Res., [Atmos.]* **2005**, *110*, 8.

(27) Rader, D. J.; McMurry, P. H. Application of The Tandem Differential Mobility Analyzer to studies of droplet growth or evaporation. *J. Aerosol Sci.* **1986**, *17*, 771−787.

(28) Cruz, C. N.; Dassios, K. G.; Pandis, S. N. The effect of dioctyl phthalate films on the ammonium nitrate aerosol evaporation rate. *Atmos. Environ.* **2000**, *34*, 3897−3905.

(29) Brechtel, F. J.; Kreidenweis, S. M. Predicting particle critical supersaturation from hygroscopic growth measurements in the

humidified TDMA. part I: Theory and sensitivity studies. *J. Atmos. Sci.* **2000**, *57*, 1854−1871.
(30) Wexler, A. S.; Seinfeld, J. H. 2nd-Generation Inorganic Aerosol Model. *Atmos. Environ. Part A:* **1991**, *25*, 2731−2748.
(31) Autho, R. *Foundation for Statistical Computing*; Vienna, Austria, 2006.
(32) Pathak, R. K.; Stanier, C. O.; Donahue, N. M.; Pandis, S. N. Ozonolysis of α-pinene at atmospherically relevant concentrations: Temperature dependence of aerosol mass fractions (yields). *J. Geophys. Res., [Atmos.]* **2007**, *112*, D03201, 10.1029/2006JD007436.
(33) Weisberg, S. *Applied Linear Regression*, 2nd ed.; John Wiley & Sons: New York, 1985.
(34) Fox, J. *Applied Regression Analysis, Linear Models, and Related Methods*; Sage Publications, Inc.: Thousand Oaks, CA, 1997.
(35) Fox, J. *An R and S-PLUS Companion to Applied Regression*; Sage Publications, Inc.: Thousand Oaks, CA, 2002.
(36) Loader, C. *Local Regression and Likelihood*; Springer: New York, 1999.
(37) Sarode, P. R.; Chetal, A. R. X-Ray Chemical-Shifts and Atomic Charges. *J. Phys. F: Met. Phys.* **1977**, *7*, 745−751.
(38) Saathoff, H.; Naumann, K. H.; Schnaiter, M.; Schock, W.; Mohler, O.; Schurath, U.; Weingartner, E.; Gysel, M.; Baltensperger, U. Coating of soot and (NH4)(2)SO4 particles by ozonolysis products of alpha-pinene. *J. Aerosol Sci.* **2003**, *34*, 1297−1321.
(39) Baltensperger, U.; Kalberer, M.; Dommen, J.; Paulsen, D.; Alfarra, M. R.; Coe, H.; Fisseha, R.; Gascho, A.; Gysel, M.; Nyeki, S.; Sax, M.; Steinbacher, M.; Prevot, A. S. H.; Sjoren, S.; Weingartner, E.; Zenobi, R. Secondary organic aerosols from anthropogenic and biogenic precursors. *Faraday Discuss.* **2005**, *130*, 265−278.
(40) Varutbangkul, V.; Brechtel, F. J.; Bahreini, R.; Ng, N. L.; Keywood, M. D.; Kroll, J. H.; Flagan, R. C.; Seinfeld, J. H.; Lee, A.; Goldstein, A. H. Hygroscopicity of secondary organic aerosols formed by oxidation of cycloalkenes, monoterpenes, sesquiterpenes, and related compounds. *Atmos. Chem. Phys.* **2006**, *6*, 2367−2388.
(41) Cziczo, D. J.; Nowak, J. B.; Hu, J. H.; Abbatt, J. P. D. Infrared spectroscopy of model tropospheric aerosols as a function of relative humidity: Observation of deliquescence and crystallization. *J. Geophys. Res., [Atmos.]* **1997**, D15.
(42) Onasch, T. B.; Siefert, R. L.; Brooks, S. D.; Prenni, A. J.; Murray, B.; Wilson, M. A.; Tolbert, M. A. Infrared spectroscopic study of the deliquescence and efflorescence of ammonium sulfate aerosol as a function of temperature. *J. Geophys. Res., [Atmos.]* **1999**, *104*, 21317−21326.
(43) Tang, I. N.; Munkelwitz, H. R. Water activities, densities, and refractive-indexes of aqueous sulfates and sodium-nitrate droplets of atmospheric importance. *J. Geophys. Res., [Atmos.]* **1994**, *99*, 18801−18808.
(44) Han, J. H.; Martin, S. T. Heterogeneous nucleation of the efflorescence of (NH4)(2)SO4 particles internally mixed with Al2O3, TiO2, and ZrO2. *J. Geophys. Res., [Atmos.]* **1999**, *104*, 35433−33553.
(45) Biskos, G.; Paulsen, D.; Russell, L. M.; Buseck, P. R.; Martin, S. T. Prompt deliquescence and efflorescence of aerosol nanoparticles. *Atmos. Chem. Phys.* **2006**, *6*, 4633−4642.
(46) Kleindienst, T. E.; Smith, D. F.; Li, W.; Edney, E. O.; Driscoll, D. J.; Speer, R. E.; Weathers, W. S. Secondary organic aerosol formation from the oxidation of aromatic hydrocarbons in the presence of dry submicron ammonium sulfate aerosol. *Atmos. Environ.* **1999**, *33*, 3669−3681.
(47) Badger, C. L.; George, I.; Griffiths, P. T.; Braban, C. F.; Cox, R. A.; Abbatt, J. P. D. Phase transitions and hygroscopic growth of aerosol particles containing humic acid and mixtures of humic acid and ammonium sulphate. *Atmos. Chem. Phys.* **2006**, *6*, 755−768.
(48) Weis, D. D. E.; G. E. Water content and morphology of sodium chloride aerosol particles. *J. Geophys. Res., [Atmos.]* **1999**, *104*, 21275−21285.
(49) Cziczo, D. J.; Abbatt, J. P. D. Infrared observations of the response of NaCl, MgCl2, NH4HSO4, and NH4NO3 aerosols to changes in relative humidity from 298 to 238 K. *J. Phys. Chem. A* **2000**, *104*, 2038−2047.
(50) Gysel, M.; Weingartner, E.; Baltensperger, U. Hygroscopicity of aerosol particles at low temperatures. 2. Theoretical and experimental hygroscopic properties of laboratory generated aerosols. *Environ. Sci. Technol.* **2002**, *36*, 63−68.
(51) Colberg, C. A.; Krieger, U. K.; Peter, T. Morphological investigations of single levitated H2SO4/NH3/H2O aerosol particles during deliquescence/efflorescence experiments. *J. Phys. Chem. A* **2004**, *108*, 2700−2709.
(52) Yu, J. Z.; Cocker, D. R.; Griffin, R. J.; Flagan, R. C.; Seinfeld, J. H. Gas-phase ozone oxidation of monoterpenes: Gaseous and particulate products. *J. Atmos. Chem.* **1999**, *34*, 207−258.
(53) Glasius, M. L.; M.; Calogirou, A.; Di Bella, D.; Jensen, N. R.; Hjorth, J.; Kotzias, D.; Larsen, B. R. Carboxylic acids in secondary aerosols from oxidation of cyclic monoterpenes by ozone. *Environ. Sci. Technol.* **2000**, *34*, 1001−1010.
(54) Raymond, T. M.; Pandis, S. N. Cloud activation of single-component organic aerosol particles. *J. Geophys. Res., [Atmos.]* **2002**, *107*.

Received for review August 18, 2006. Revised manuscript received November 28, 2006. Accepted January 19, 2007.

ES0619915

Supplemental Section

S1. Calculation of Bulk volume fraction

From our observed values of total volume, V_T, we estimate a bulk first-order loss rate coefficient, $\bar{k}$, from fitting the data for an extended period in which we expect deposition to be the dominant loss mechanism in the chamber:

$$\ln V_T = b + \bar{k}t \qquad \ldots(1)$$

In equation (1), t is time and b is an arbitrary intercept term. From this method we estimate the value of $\bar{k}$ and apply this loss rate to the ammonium sulfate volume concentration observed at the time just preceding the onset of ozonolysis reactions. This extrapolation allows us to estimate the ammonium sulfate and SOA fractions of the total aerosol as they are lost to the walls of the Teflon bag (*1*).

S2. Calculation of size-resolved volume fraction

In our model, we use a sectional representation with moving size bins to simulate condensation and deposition processes occurring in the smog chamber; coagulation is neglected as the characteristic time scales (on the order of days) for this process are considerably longer than the duration of our experiments (a few hours) (*2*).

We begin with a volume balance for the bulk particle volume, V_T:

$$\frac{dV_T}{dt} = \frac{d}{dt}\left(\sum_i N_i V_{p,i}\right) = \sum_i N_i \left(\frac{dV_{p,i}}{dt}\right) + \sum_i V_{p,i}\left(\frac{dN_i}{dt}\right) \qquad \ldots(2)$$

t is time, N_i and $V_{p,i}$ are the number concentration and single particle volume of a particle of size class i, respectively. The right-hand side of the equation is simply derived from the chain rule, but in our model we assume that condensation is the only mechanism by which the aerosol volume changes and deposition to the walls is the only mechanism by which the number concentration is altered.

The rate of change of volume of a single particle of size i is equal to the net flux to of condensable species A to the particle:

$$\frac{dV_{p,i}}{dt} = J_i \rho_A^{-1} M_A \qquad \ldots(3)$$

ρ_A and M_A and are the density and molecular weight of species A, respectively; the flux or molecular velocity term J_i in the transition regime can be expressed as

$$J_i = \left(\frac{1 + Kn_i}{1 + 1.71Kn_i + 1.33Kn_i^2}\right) 2\pi D_{AB} D_{p,i} (c_\infty - c_{s,i}) \qquad \ldots(4)$$

$D_{p,i}$ is the diameter of a particle of size class i, Kn_i is the Knudsen number ($\lambda/D_{p,i}$), D_{AB} is the molecular diffusivity of species A in air, $c_{s,i}$ is the saturation vapor pressure over the particle and c_∞ is the bulk gas-phase concentration of species A.

The change in number concentration arises from deposition of particles to the chamber walls and is modeled as a first-order loss process:

$$\frac{dN_i}{dt} = -k_i N_i \qquad \ldots(5)$$

k_i is the first-order loss coefficient for particles of size i. For our calculations, the loss rate is assumed to be independent of size ($k_i = \bar{k}$), and the bulk loss coefficient, $\bar{k}$, is calculated by equation (1).

Equations 2-5 provide a framework for simulating the chemical and physical processes occurring in the smog chamber but require inputs of several parameters: ρ_A and M_A in equation (3), and parameters D_{AB} and $c_{s,i}$ for the diffusion model in equation (4). The bulk gas-phase concentration c_∞ is used as a fitting parameter to reproduce the change in total particle volume, dV_T/dt. dV_T/dt is determined by fitting a piece-wise cubic equation to the observed values of $V_T(t)$ and differentiating with respect to time.

For ρ_A and M_A we use values for pinonic acid, the most prevalent component in α-pinene and limonene SOA. For the diffusion coefficient D_{AB} in equation (4), we use an estimate based on the semi-empirical approach of Fuller et al. (*3*), again using pinonic acid as our reference compound. The size-dependent equilibrium vapor pressure $c_{s,i}$ we estimated from the Kelvin equation:

$$c_{s,i} = c_s^0 \exp\left(\frac{4\sigma M_A}{RT\rho_A D_{p,i}}\right) \qquad \ldots(6)$$

M_A and ρ_A are the molecular weight and density, and we use the values for pinonic acid. c_s^0 is the saturation vapor pressure of the pure organic component over a flat surface and σ is the surface tension. In our conceptual model, we assume that the solid ammonium sulfate core is coated by an organic liquid-phase so the parameters that characterize this effect are dependent only on the organic phase without consideration for mixture effects. c_s^0 and σ are constrained by values considered reasonable for the condensable species formed. We used values between 0.14 and 1.05 ppb for c_s^0 and between 0.017 and 0.043 J/m^2 for σ. σ for DOP is 0.033 J/m^2 (*4*). Table S1 lists the range of values used for each of the other relevant parameters introduced above.

Equations 2-6 were integrated explicitly in time with the Euler method; a step size was chosen by testing increasingly smaller values for the time step until the solutions to the equations no longer changed within a reasonable margin of error. A time-step of 0.1 hour was determined to be sufficiently accurate for this study. After obtaining the numerical solutions to the equations, we can estimate the volume of SOA for each size bin:

$$V_{SOA}\left(D_{p,i}\right) = \frac{\pi}{6}\left(D_{p,i}^3 - D_{p0,i}^3\right) \qquad \ldots(7)$$

$D_{p0,i}$ is the initial diameter and $D_{p,i}$ is the final diameter after growth.

An example of model output and measured size distribution is shown in Figure S1. The fit of the model was assessed using the mean normalized error (*4*) of particle volume concentration for each size bin between 80 and 400 nm (Table S2). Errors outside of this size range are biased by size bins with a negligible count of particles and are therefore not included in the calculation of the mean normalized error.

S3. Estimation of inflection point by local regression

Local regression is a data-smoothing technique that can be used to explore features in a data set without imposing a predetermined global parametric structure to the fitting model. We use this technique to approximate the growth factor curve with a smooth function; an inflection point in the smooth curve is taken as a possible indication of a vertical discontinuity in the original data. Fitting of the local regression model is implemented through the *locfit* library in R (*5*), and is described in detail in the monograph by Loader (*6*). Briefly summarizing, we use the observations for growth factor (*GF*) and relative humidity (*RH*) for each point *i* to fit a regression model of the form (lower case notation used to represent specific values of the random variables):

$$gf_i = \mu(rh_i) + \varepsilon_i$$

where $\mu(rh)$ is an unknown function and ε_i is the error term representing the non-deterministic component of the size measurements (e.g., instrument noise, errors in inversion of scanning DMA data, peak-fitting errors). We approximate $\mu(rh)$ by a quadratic function using only those points contained within a smoothing window (rh–$b(rh)$,rh+$b(rh)$), defined by the bandwidth $b(rh)$. The value of $\mu(rh)$ is then estimated by the first polynomial coefficient, a_0, obtained from minimizing the following objective function (*6*):

$$\sum_{i=1}^{n}\left[1-\left(\frac{rh_i - rh}{b(rh)}\right)^3\right]^3\left[gf_i - \left(a_0 + a_1(rh_i - rh) + \frac{1}{2}a_2(rh_i - rh)^2\right)\right]^2$$

A tricube weight function is applied to the square of the residuals to assign largest weights to observations closest to rh (*6*).

An example of this fit and its derivative estimate applied to Experiment L5 is shown in Figures S2a and b, respectively. In each of our fitting routines, we choose a constant bandwidth [$b(rh) = b$] with b chosen between 5 and 15 % RH, depending on sampling intervals of RH and total number of measurements for each experiment. In most cases, where the sampling range and frequency of RH are sufficiently large, the choice of bandwidth does not affect the location of the inflection point. The inflection points estimated for all experiments are shown in Figure S2c; these estimates are comparable within uncertainty to the effective ERH calculated by the logistic regression procedure outlined in the main text.

S4. Example size distributions

Example size distributions near the effective ERH are shown in Figure S3. The effective ERHs for Experiment A3 (Figure S3a) and Experiment L2 (Figure S3b) are 30 and 29%, respectively, and significant shifts in the size distributions can be observed with small decreases in RH near these points. For experiments with higher SOA loadings (e.g., Experiments L4 and L5), low growth factors lead to less apparent size transitions (as shown in Figure S2a for Experiment L5) and we rely on statistical inference to estimate the ERH.

References

(1) Pathak, R. K.; Stanier, C. O.; Donahue, N. M.; Pandis, S. N. Ozonolysis of α-pinene at atmospherically relevant concentrations: Temperature dependence of aerosol mass fractions (yields). *submitted* **2006**.
(2) Cocker, D. R.; Flagan, R. C.; Seinfeld, J. H. State-of-the-art chamber facility for studying atmospheric aerosol chemistry. *Environ. Sci. Technol.* **2001**, *35*, 2594-2601.
(3) Fuller, E. N.; Schettle.Pd; Giddings, J. C. A New Method for Prediction of Binary Gas-Phase Diffusion Coeffecients. *Industrial and Engineering Chemistry* **1966**, *58*, 19-&.
(4) Seinfeld, J. H.; Pandis, S. N. *Atmospheric Chemistry and Physics: From Air Pollution to Climate Change*; 2nd ed.; John Wiley & Sons: New York, 2006.
(5) R Development Core Team. *R: A Language and Environment for Statistical Computing*; R Foundation for Statistical Computing: Vienna, Austria, 2006.
(6) Loader, C. *Local Regression and Likelihood*; Springer: New York, 1999.
(7) Bilde, M.; Pandis, S. N. Evaporation rates and vapor pressures of individual aerosol species formed in the atmospheric oxidation of alpha- and beta-pinene. *Environ. Sci. Technol.* **2001**, *35*, 3344-3349.
(8) Capouet, M.; Muller, J. F. A group contribution method for estimating the vapour pressures of alpha-pinene oxidation products. *Atmospheric Chemistry And Physics* **2006**, *6*, 1455-1467.

Tables

Table S1. Condensation model parameter description and values

Parameter	Description	Value or Range of Values	Comment
ρ_A	Density	1.2 g cm^{-3}	
M_A	Molecular weight	184 g mol^{-1}	Molecular weight of pinonic acid.
D_{AB}	Diffusivity	0.06 cm^2 s^{-1}	Calculated for pinonic acid by method of Fuller et al. (*3*).
c_∞	Bulk gas-phase concentration	10-50 ppbC	Fitted parameter; calculated during simulation.
c_s^0	Surface vapor pressure	0.14-1.05 ppb	Bilde and Pandis (*7*) estimates 0.7 ppb for pinonic acid; Capouet and Muller (*8*) estimates a value an order of magnitude higher from group contribution calculations.
Σ	Surface tension	0.017-0.043 J m^{-2}	Surface tension of DOP is 0.033 J/m^2 (*4*).
T	Temperature	298 K	Standard temperature.
$\bar{k}$	First-order wall loss coefficient	0.16-0.38 hr^{-1}	

Table S2. Data Analysis Calculations and Modeling Results.

Experiment Name	Bulk SOA volume fraction	Size-resolved SOA volume fraction	Mean error of model fit† (% volume)	Effective ERH (%)
L1	0.33	0.59	16	32.7 ± 2.3
L2	0.40	0.73	17	28.9 ± 2.6
L3	0.55	0.87	19	33.2 ± 2.8
L4	0.73	0.88	43	33.4 ± 3.3
L5	0.81	0.94	43	29.8 ± 3.2
A1	0.41	0.54	17	29.4 ± 2.2
A2	0.46	0.72	14	30.6 ± 1.4
A3	0.49	0.63	12	29.7 ± 1.9

†between 80 and 400 nm

Figures

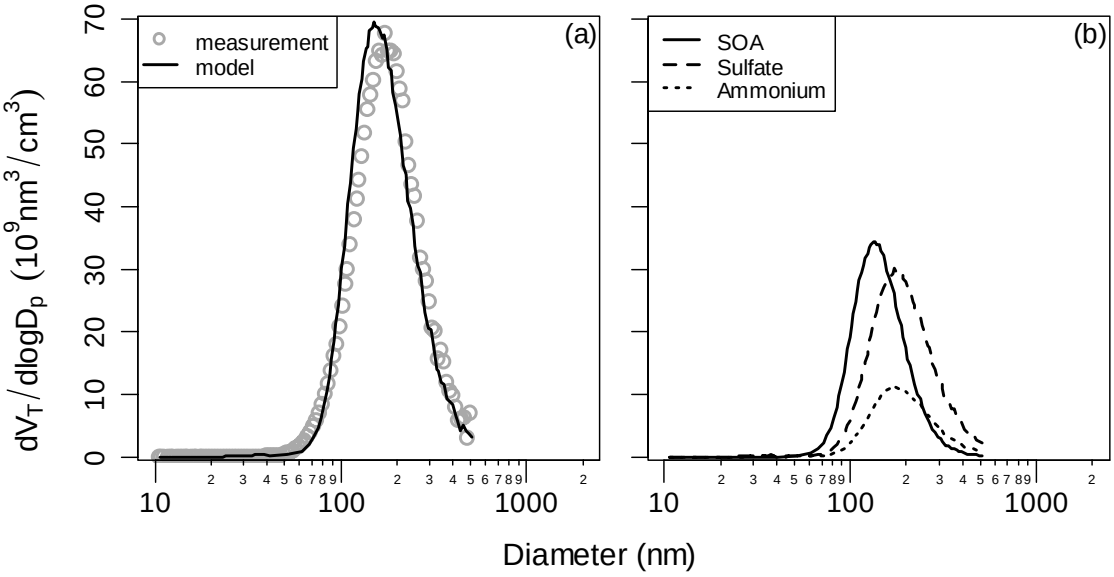

Figure S1. An example comparison of modeled size distribution and measurement taken by the SMPS (Figure S1a), and organic aerosol loading on ammonium sulfate seed calculated by the model (Figure S1b). Figures shown are for Experiment A1, 127 minutes after α-pinene injection.

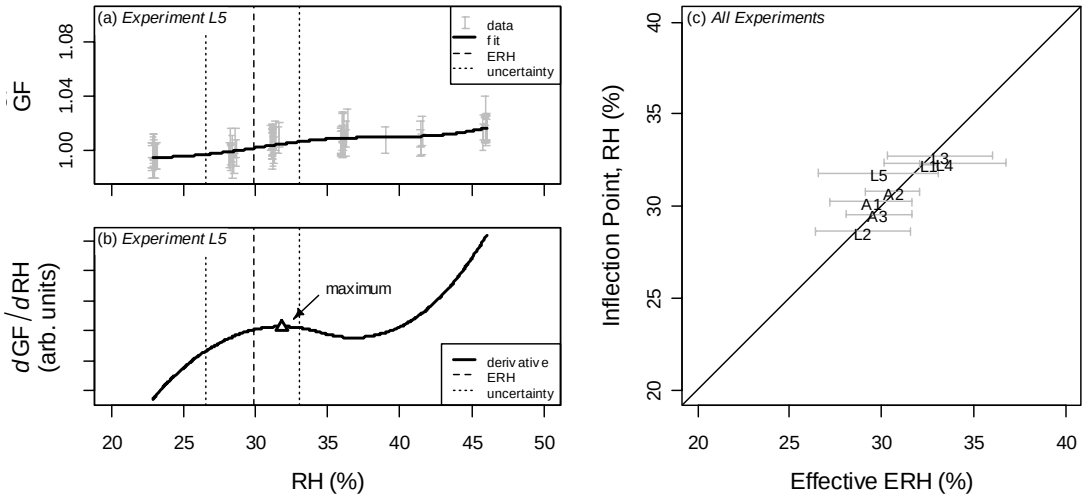

Figure S2. (a) Local regression model fitted to measurements (vertical bars indicating uncertainty in GF) in which the RH in the HTDMA was in equilibrium, (b) first derivative of the local regression curve with a maximum at 32% RH, and (c) scatterplot of inflection points and effective ERH (horizontal bars span RHs corresponding to 5th and 95th percentile of efflorescence probability estimates).

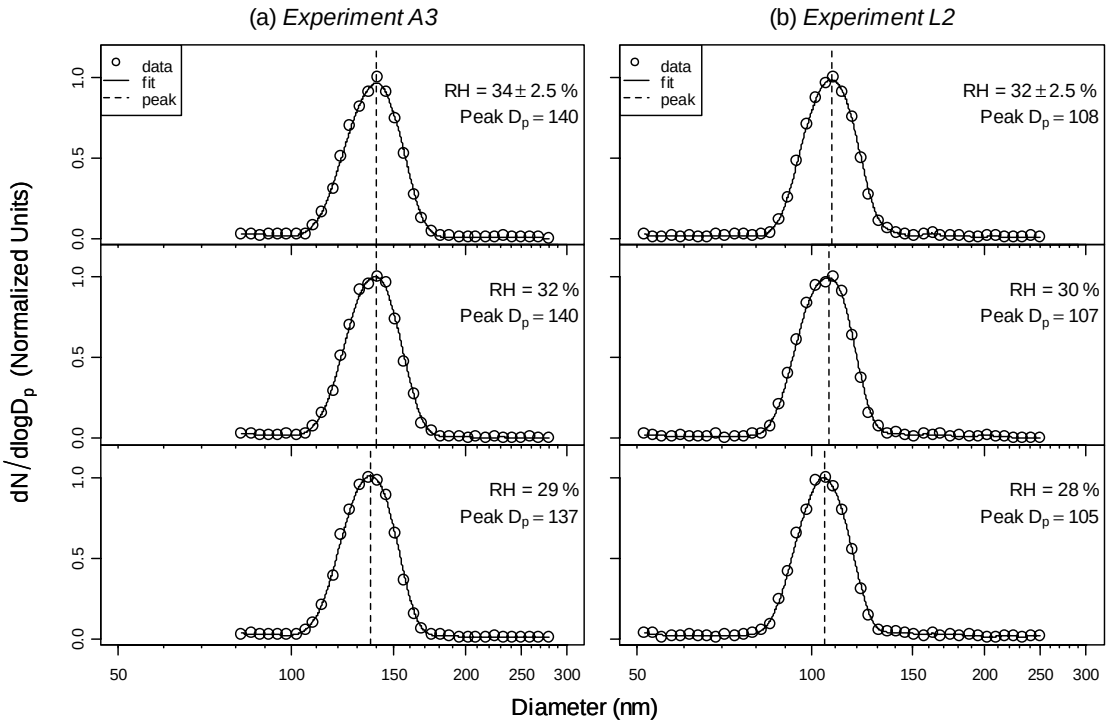

Figure S3. Size distributions as a function of RH for (a) Experiment A3 and (b) Experiment L2.